



Pergamon

Acta Materialia 50 (2002) 4431–4447



www.actamat-journals.com

Microstructure evolution in pearlitic steels during wire drawing

Michael Zelin *

The Goodyear Tire & Rubber Company, Technical Center, PO Box 3531, Akron, OH 44309-3531, USA

Received 9 April 2002; accepted 28 June 2002

Abstract

Major processes affecting microstructure of a drawn pearlitic wire including lamellae thinning, changes in inter-lamellar interface and metallographic and crystallographic texture, plastic flow localization, and dynamic strain aging were characterized. Heavily drawn pearlite represents a nano-composite with thickness of ferrite and cementite lamellae decreasing during wire drawing. Volume fraction of inter-phase interfaces is comparable with that of pearlitic cementite and they are associated with high elastic stresses. Stretching and rotation of pearlite colonies result in their alignment with the wire axis. This is accompanied by increase in a local ductility at the true strain below from 1.5 to 2 and then decrease at higher strain levels. Development of a strong crystallographic texture causes anisotropy in mechanical properties. Targeted observations of plastic flow at the same region showed two systems of localized shear bands and provided information on their development. A dramatic decrease in elongation to failure in wires after drawing is linked to the existence of the localized shear bands. Dynamic strain aging increases strength and degrades ductility of drawn wires. © 2002 Acta Materialia Inc. Published by Elsevier Science Ltd. All rights reserved.

Keywords: Plastic flow; Microstructure; Pearlite; Ferrite; Cementite

1. Introduction

Quest for improved processing and service properties of pearlitic steels, a widely used group of industrial materials, motivated in-depth studies [1–22] of deformation behavior of ferrite. Fig. 1(a) illustrates structure of lamellar pearlite consisting of ferrite and cementite plates. Development of high strength steel wires, particularly, for tire cord applications [23–26], exemplifies importance of

such a fundamental understanding of pearlite deformation. Microstructural changes occurring during wire drawing can result in a record strength comparable with that of a quenched steel (Fig. 1b).

This paper deals with the following processes occurring in pearlitic steels during wire drawing:

- lamellae thinning;
- evolution of lamellae interfaces;
- texture changes;
- metallographic texture;
- crystallographic texture;
- plastic flow localization;
- dynamic strain aging.

* Tel.: +1-330-796-6934; fax: +1-330-796-3947.

E-mail address: michael.zelin@goodyear.com (M. Zelin).

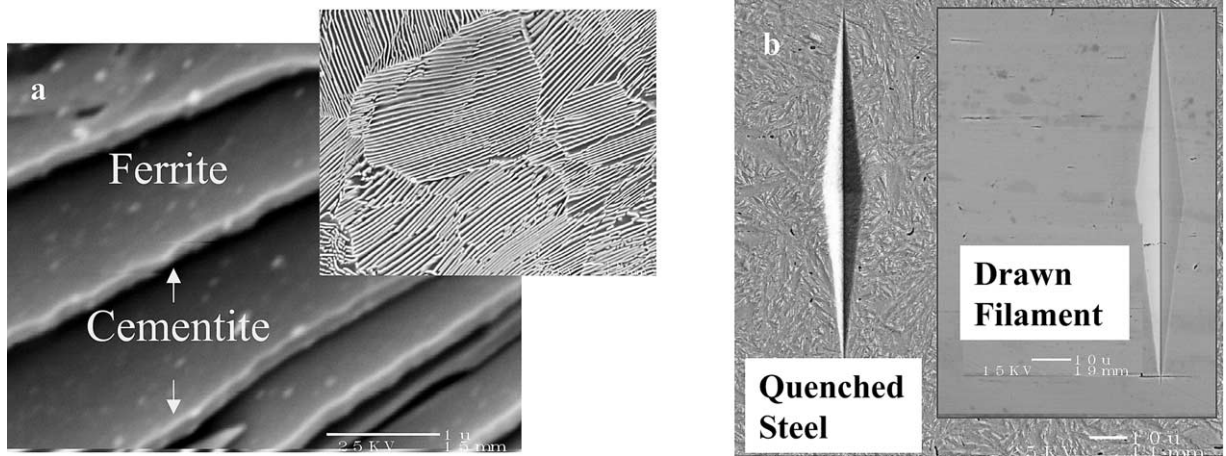


Fig. 1. (a) Pearlite in a patented steel wire; an insert shows pearlite colonies. (b) Micro-hardness indentations imprinted in a quenched steel wire with a martensitic microstructure and a drawn pearlitic steel filament. SEM.

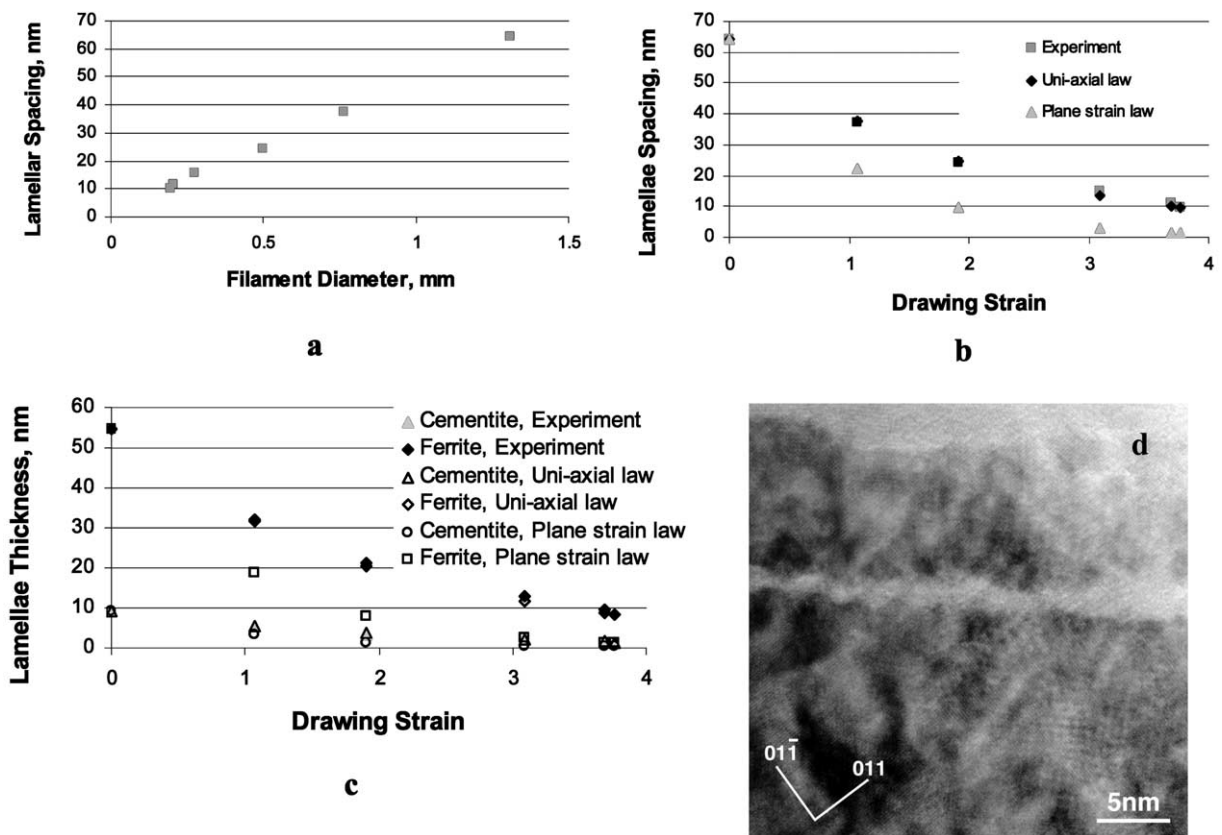


Fig. 2. (a) Inter-lamellar spacing as a function of filament diameter and (b) drawing strain. (c) thickness of ferrite/cementite lamellae as a function of drawing strain [28], and (d) HRTEM of a drawn pearlitic steel [30].

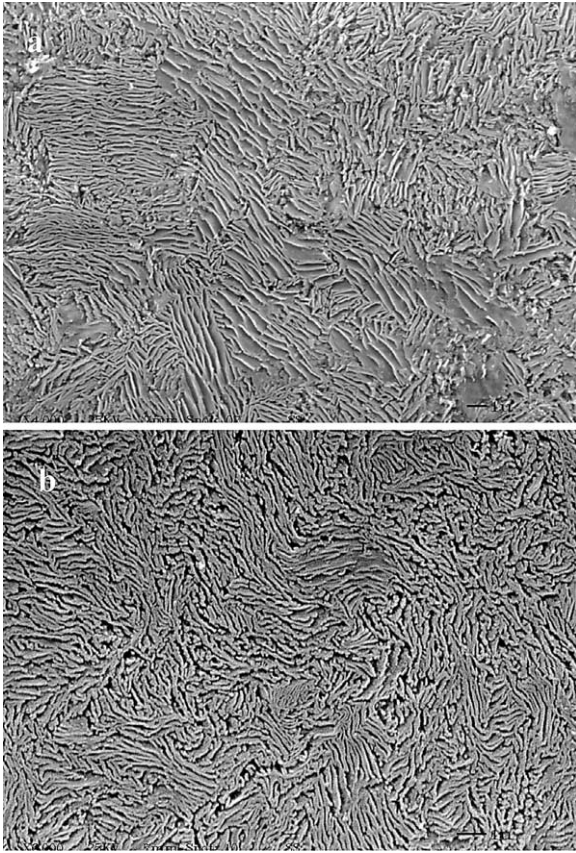


Fig. 3. Pearlitic structure at a normal cross-section of wires drawn to a true strain of (a) 0.31 and (b) 1.83. SEM.

Experimental data characterizing these processes are presented and effect of these processes on mechanical characteristics of drawn wires is discussed.

2. Experimental procedure

Experiments were performed on high carbon steel wires with carbon content ranging from 0.8 through 0.96%, both commercially and laboratory processed to obtain a fine pearlitic microstructure. Processing included patenting, brass plating, and fine wire drawing in a wet drawing machine. Tensile tests were conducted in an Instron testing machine, and torsion tests were performed in an ATM torsion tester. To examine anisotropy of

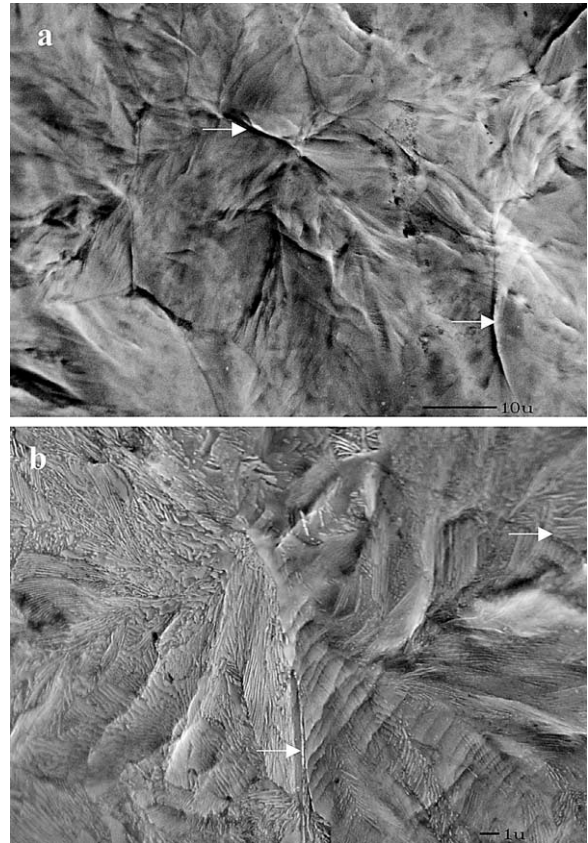


Fig. 4. Deformation of (a) former austenite grains and (b) pearlite globular. Arrows indicate former austenite boundaries. SEM.

drawn wires, Knoop micro-hardness measurements were performed on the longitudinal cross section of drawn filaments with the orientation of the long diagonal parallel and perpendicular to the filament axis. Additionally, shape of diamond conical indenter imprinted with a Rockwell hardness tester on the longitudinal cross section of as-patented wires and highly drawn wires was examined.

Microstructural examinations were performed on wires drawn to successive strain levels. Standard mounting and polishing procedures were used for preparation of samples for microstructural observations on longitudinal wire cross section and normal to the wire axis cross section. Samples were picral etched. For studying material flow, deformation relief resulted from wire drawing was examined in a scanning electron microscope

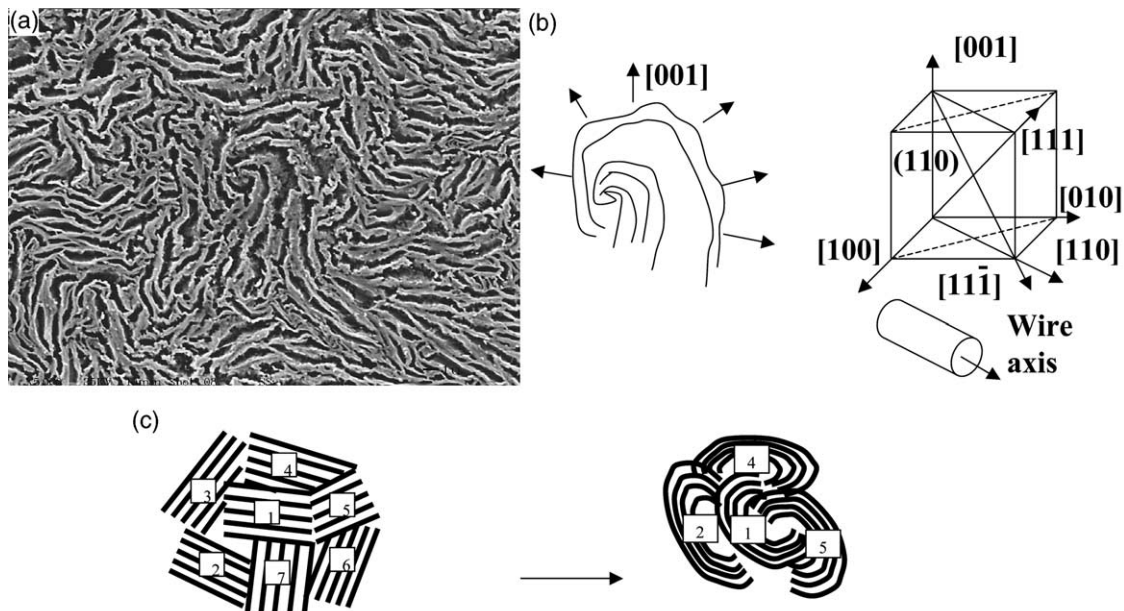


Fig. 5. (a) Wavy pearlitic structure at a normal cross section of a drawn wire. (b) and (c) are schematic diagrams illustrating crystal orientation in a heavily drawn wire with a [110] fiber texture and possible changes in a number of neighboring pearlite colonies due to bending and stretching, respectively. SEM.

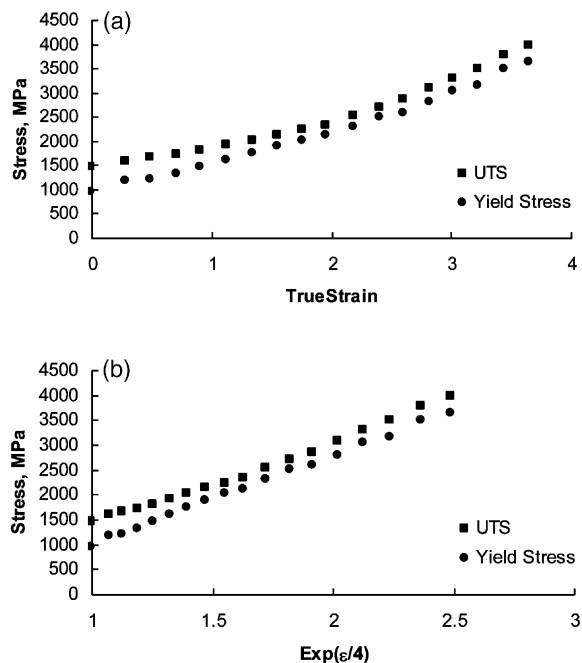


Fig. 6. Typical for pearlitic steel wires dependence of (a) yield stress (Y.S.) and ultimate tensile stress (UTS) as a function of drawing strain and (b) as a function of $\text{exp}(\epsilon/4)$.

(SEM). A region with approximate dimension of $10 \times 0.8 \text{ mm}^2$ was pre-polished before deformation, and markers were imprinted at the polished surface by using a Knoop micro-hardness diamond indenter to locate the same area after wire drawing. Wires were drawn with 20% drawing strain in one pass, and SEM micrographs were taken from the same wire area at the total strain of 20, 40 and 60%.

Atomic force microscopy (AFM) was also used to examine etched microstructure of drawn filaments. Observations were performed in a tapping mode. To examine aging effects, differential scanning calorimetry tests were performed on fine drawn filaments. Additionally, ABAQUS, a general purpose finite element method (FEM) code, was used in computer simulations of pearlite deformation during wire drawing.

3. Lamellae thinning

In isotropic uni-axial tension, axial stretching of a colony with an original interlamellar spacing, S_0 , and Miller indexes h_0 , k_0 , and l_0 , defining its orien-

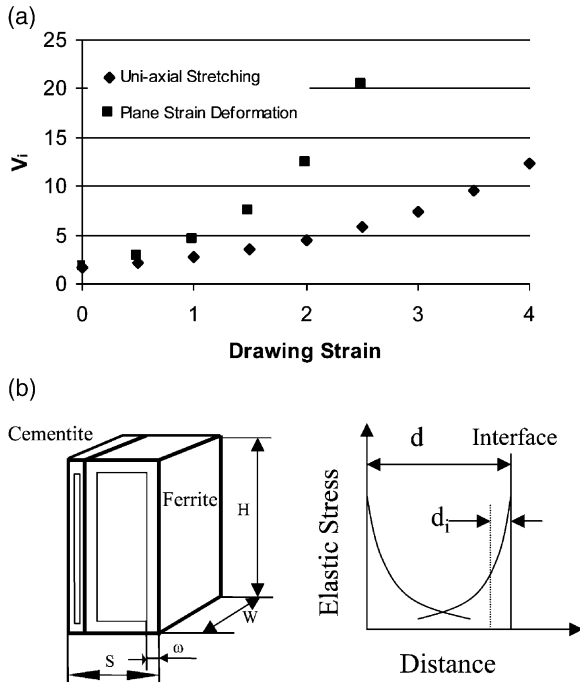


Fig. 7. (a) Volume fraction of ferrite/cementite interfaces as a function of drawing strain, (b) and (c) are schematic diagrams illustrating geometry of ferrite/cementite interfaces and elastic stress around them, respectively.

Here $k_1 = 1$, $k_2 = 1$, and $k_3 = -2$ for uni-axial tension characterizing relationship between macroscopic strain components in wire drawing, and $k_1 = 2$, $k_2 = 0$, and $k_3 = -2$ for plane strain deformation occurring in bcc-materials with an axial [110]-texture developed during wire drawing [27].

With increasing drawing strain, pearlite colonies become aligned with the wire axis (see below), and Eq. (1) can be simplified to the following form:

$$S = S_0 \exp(-k\epsilon/2) \quad (2)$$

where, $k = 1$ for uni-axial stretching and $k = 2$ for plane strain stretching.

Fig. 2(a) shows pearlite interlamellar spacing measurements [28] in a pearlitic wire drawn to different diameters, D . Linear dependence between S and D is consistent with direct proportionality between interlamellar spacing and wire diameter: $D = NS$, assumed by uni-axial stretching. N -value of 2×10^4 is in a good agreement with the number of pearlite plates along the wire diameter estimated from the original wire and pearlite lamellae dimensions.

Assuming that both ferrite plates and cementite plates undergo the same strain, the expressions analogous to Eq. (2) can be obtained for thickness

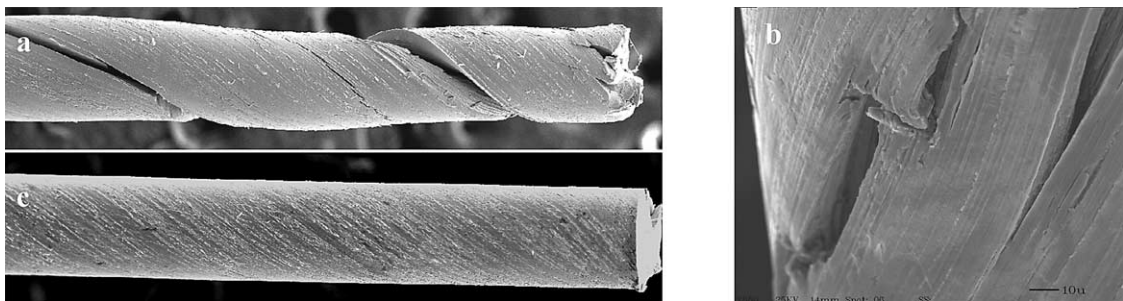


Fig. 8. (a, b) Delaminated filament and (c) filament that showed stable torsion behavior (produced with a use of a small final pass reduction [37]). SEM.

tation with respect to the wire axis coinciding with the z -axis is accompanied by the decrease of interlamellar spacing, S , according to the following expression [4]:

$$S = S_0 / (h_0^2 \exp(k_1 \epsilon) + k_0^2 \exp(k_2 \epsilon) + l_0^2 \exp(k_3 \epsilon))^{0.5} \quad (1)$$

of ferrite plates, S_f , and cementite plates, S_c . Fig. 2(b) and 2(c) demonstrate a good consistency between results of experimental measurements of interlamellar spacing and thickness of ferrite and cementite plates [28] and predictions assuming uni-axial stretching of pearlite [1,4,5,7]. In a highly drawn wire, thickness of ferrite and cementite

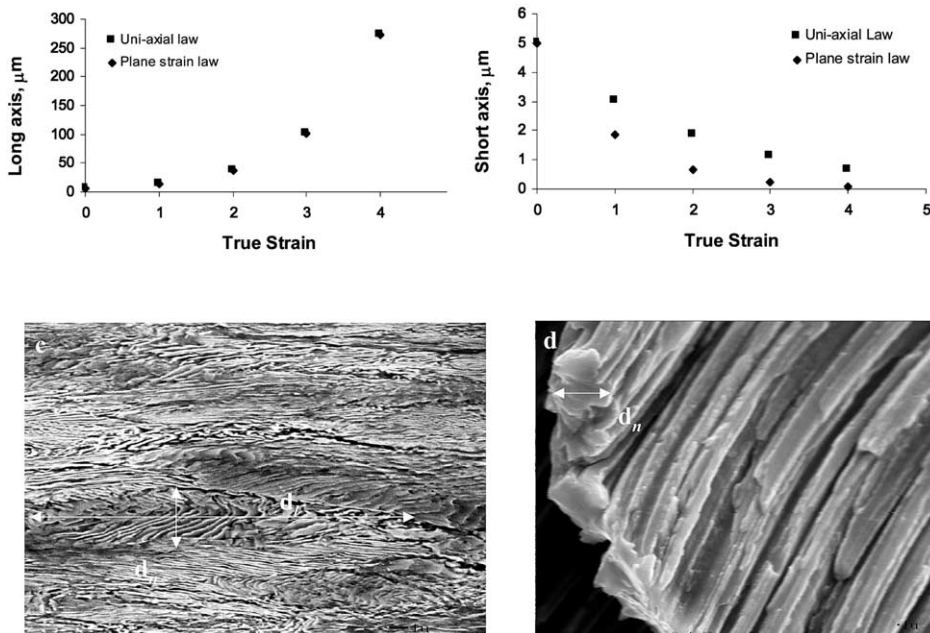


Fig. 9. (a) Length of pearlite colony parallel to the wire axis, d_l , and (b) normal to the wire axis, d_n , as a function of drawing strain. (c) and (d) show drawn pearlite. SEM.

plates is approximately 10 and 2 nm (Fig. 2c), or assuming lattice parameter of 2.8 Å for ferrite and 4.5 Å for cementite [29] is approximately 40 atoms and 5 atoms, respectively. Such a small thickness of ferrite/cementite plates has an important effect on properties of heavily drawn wires, especially, torsion behavior (see below). Thickness of ferrite/cementite plates observed on a high resolution TEM micrograph [30] shown in Fig. 2(d) is in a good agreement with predictions based on the assumption of uni-axial tension.

While model predictions assuming plane strain deformation of pearlite are not supported by the S , S_f , and S_c measurements, they are consistent with a whirled appearance of pearlite plates on the normal cross section to the wire axis [5,22,26]. Fig. 3(a) and 3(b) illustrate that originally straight pearlite plates become wavy after drawing. The swirled appearance of pearlite plates becomes more pronounced with increased drawing strain. Some data reported by Glenn et al. [3] and Langford [4,5] also support plane strain deformation of pearlite. Langford [5] attributed an apparent contradiction between plane strain-like deformation of pearlite

as observed on the normal cross section and uni-axial like thinning of pearlite lamellae measured on longitudinal wire cross section to the difference in deformation of pearlite colonies with different spatial orientation and strain localization. In addition to these factors supported by experimental observations (see below), the following considerations can also explain apparent contradiction between expected plane strain like deformation [27] for a [110] fiber textured steel wire [11] and uni-axial like thinning of pearlite colonies:

- (i) It is possible that a structure of pearlite globulars or cementite lamellae with an orthorhombic crystal structure acting as a reinforcement within ferrite matrix cause uni-axial character of pearlite deformation. Fig. 4 illustrates that pearlite colonies within former austenite grains (Fig. 4a) and within pearlite globulars (Fig. 4b) deform together.
- (ii) Fig. 5(a) shows a normal cross section of a drawn wire, and Fig. 5(b) schematically illustrates that bending of pearlite colonies results in a radial orientation of [001] direction. Only two

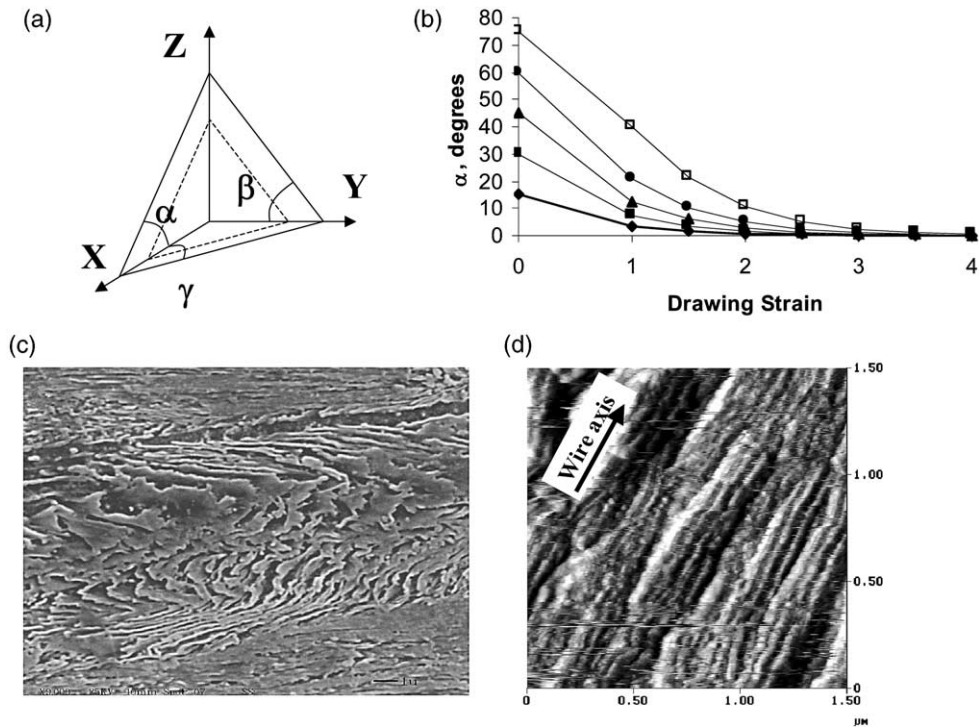


Fig. 10. (a) A schematic diagram illustrating angles between ferrite/cementite plates and coordinate axes; (b) changes in α -angle determining orientation of pearlite colony with respect to the wire axis as a function of drawing strain predicted by the uni-axial stretching law for plates with different original orientations. (c) Shows buckled pearlite colonies normal to the wire axis (SEM), and (d) shows alignment of pearlite colonies along the wire axis (AFM).

close packed directions $[111]$ and $[11\bar{1}]$ contribute to the wire stretching [27] as defined by the projection on the wire axis parallel to the $[110]$ direction and wire diameter reduction as defined by the projection on $[001]$ direction coinciding with a radial direction. Bent lamellae will deform similarly to a tube under uni-axial tension. Sub-grain boundaries can form to accommodate misorientation of neighboring cells. Langford [5] reported such sub-grain boundaries observed at the normal cross section of pearlite colonies. It is interesting to note that a combination of bending and stretching of pearlite colonies can cause topological changes that are not described by well established elementary topological transformations I and II [31]. As an example, Fig. 5(c) schematically illustrates that a number of neighboring pearlite colonies can change: colony indicated by the numeral 1 which originally had six neighboring colonies

has only three neighboring colonies after deformation.

Correct determination of character of lamellae thinning is important for predicting strength of drawn wires. Fig. 6(a) shows that true drawing strain of 4 results in an almost three fold strength increase. Fig. 6(b) indicates linear dependence of yield stress (Y.S.) and ultimate tensile strength (UTS) on $\exp(\epsilon/4)$ [1,4,5] that is consistent with uni-axial stretching model combined with a Hall–Petch dependence [32,33].

4. Evolution of interphase interfaces

While the volume of the entire wire is constant, its surface area increases with strain. For a pearlite colony, both volume fraction, V_i , and surface area, A_i , of lamellae boundaries increase with strain

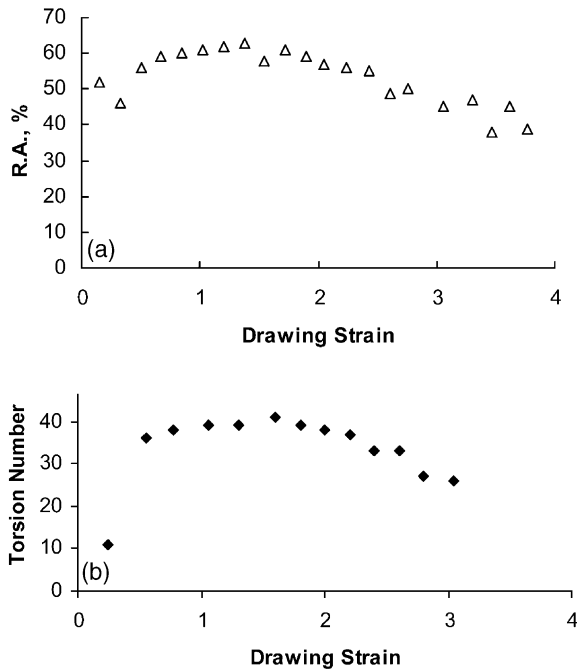


Fig. 11. (a) A typical for pearlitic steels dependence of reduction area (R.A.) and (b) number of twists before failure as a function of drawing strain.

increase. Sevillano et al. [7] considered grain boundary surface area increase under different stress–strain conditions. Assuming a plate-like shape of ferrite and cementite lamellae and taking into account that lamellae width and length are significantly larger than their thickness (Fig. 7), volume fraction of lamellae interfaces can be estimated as:

$$V_i = 2\omega \exp(k\varepsilon/2)/S_0 \quad (3)$$

where ω is a half thickness of cementite/ferrite interface.

Fig. 7a shows dependence of V_i as a function of drawing strain for uni-axial and plane strain conditions. For the case of uni-axial tension giving a lower estimate, a typical drawing strain of 3.6 results in almost one order of magnitude increase in V_i reaching approximately 12% comparable with volume fraction of cementite and indicating that interfaces can be considered as another phase. Note that Hidaka et al. [34] reported volume fraction of interfaces in a mechanically milled steel from 30

to 50%. Deformation of pearlite colonies also results in change of the nature of interlamellar interfaces. In as-patented wire, interfaces are coherent or semi-coherent boundaries because of special orientation relationships between ferrite and cementite also defining habit plane [29,35]. Experimentally observed $\langle 110 \rangle$ orientation of ferrite/cementite interfaces is not consistent with generally accepted orientation relationships [29]. This indicates that ferrite/cementite interfaces become non-special boundaries. Additionally, operation of $\langle 111 \rangle \{110\}$ slip systems in ferrite and $\{100\}$ slip systems in cementite causes accumulation of misfit dislocations at the interfaces leading to high elastic stress. Results of neutron diffraction measurements reported by Van Acker et al. [13] indicate that the interlamellar stresses can be as high as 2000 MPa.

To estimate thickness of the region affected by the elastic stress, drawn wires were annealed for different times. Short annealing times caused some increase in materials strength due to static aging processes [15]. At longer annealing times, wire strength stabilizes at the strength level of 0.95% of the original level. To incorporate effect of elastic stress spreading at the distance, d_i , from interfaces with spacing d (Fig. 7c), Hall–Petch [32,33] dependence can be modified as:

$$\sigma = \sigma_0 + K(d - d_i)^{-1/2} \quad (4)$$

Assuming that there is no lamellae coarsening, lamellae segmentation, or recovery processes, strength decrease can be attributed to the decrease in d_i/d -value which can be estimated as:

$$d_i/d = 1 - (1 - \delta\sigma/(\sigma - \sigma_0))^2 \quad (5)$$

where, $\delta\sigma$ is strength loss after annealing and σ is strength of as-drawn wire.

Rough estimate of thickness of the region with high elastic stress according to Eq. (5) yields approximately 0.1 d . With decreasing lamellar thickness, elastic stresses from two opposing interphase boundaries overlap. Resulting high level of elastic stresses can be a reason for brittleness of heavily drawn wires. Specifically, high elastic stresses from lamellar interfaces combined with macroscopic residual stresses caused by wire drawing can be one of the factors causing axial cracking

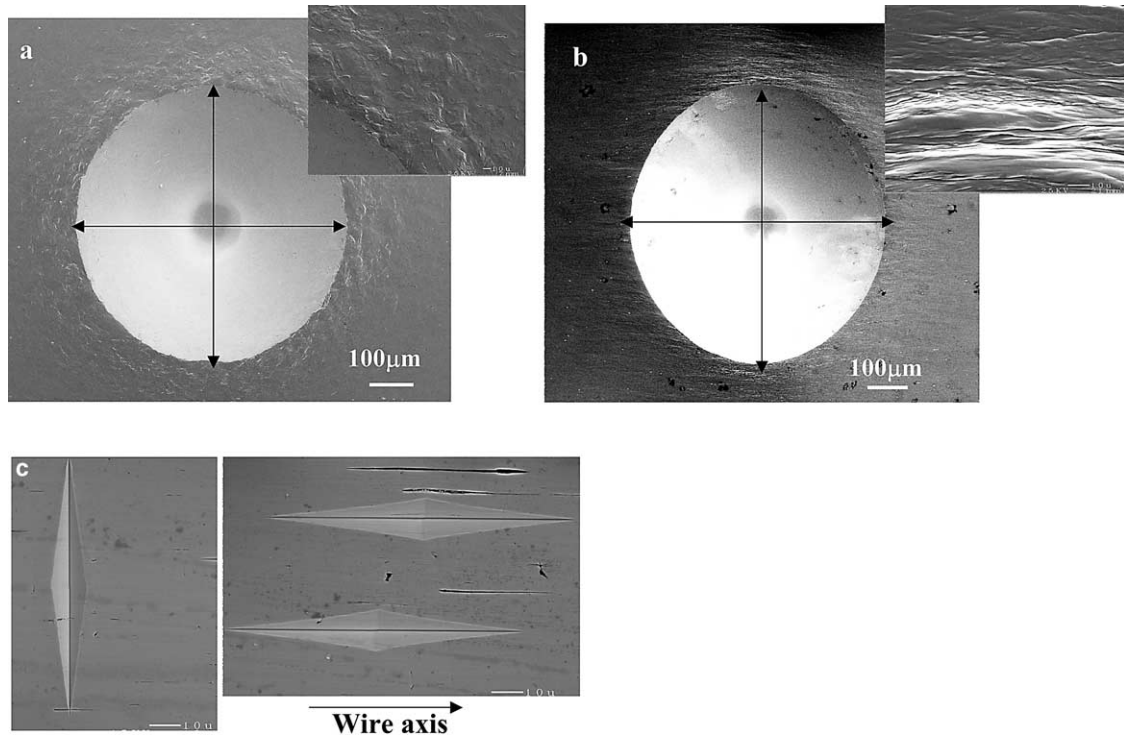


Fig. 12. Indentations imprinted at the pre-polished surface of (a) as-patented wire and (b) drawn wire by using a cone indenter, and (c) by using a Knoop diamond pyramid along and normal to the wire axis. Inserts in (a) and (b) show details of shear surfaces around the indentations. SEM.

of heavily drawn wires during torsion (Fig. 8), so called delamination [10]. Details on mechanism of delamination and effect of processing conditions are considered elsewhere [36].

5. Texture development

5.1. Metallographic texture

Metallographic texture, highly elongated pearlite colonies, develops as a result of their stretching and rotation towards the wire axis. Fig. 9(a) and 9(b) show dependence of length of a long axis and short axis of a pearlite colony (Fig. 9c) as a function of drawing strain predicted by the uni-axial stretching law and plane strain deformation law, respectively. Even though it is difficult to determine size of pearlite colonies in a highly drawn wire (Fig. 9d), overall dimensions of observed

microstructural elements are consisted with predictions of uni-axial stretching law.

During drawing, pearlite colonies align themselves along the wire axis. Assuming rotation of pearlite colony due to elongation imposed by the wire length increase, the following relationship for the angles α , β , and γ (Fig. 10a) can be obtained:

$$\operatorname{tg} \alpha = \operatorname{tg} \alpha_0 \exp(-k_\alpha \varepsilon) \quad (6a)$$

$$\operatorname{tg} \beta = \operatorname{tg} \beta_0 \exp(-k_\beta \varepsilon) \quad (6b)$$

$$\operatorname{tg} \gamma = \operatorname{tg} \gamma_0 \exp(-k_\gamma \varepsilon) \quad (6c)$$

Here, $k_\alpha = 1.5$, $k_\beta = 1.5$, and $k_\gamma = 0$ for uni-axial tension, and $k_\alpha = 2$, $k_\beta = 0$, and $k_\gamma = 1$ for plane strain conditions.

Fig. 10(b) demonstrates dependence of α -angle characterizing orientation of a pearlite colony with regard to the wire axis as a function of drawing strain for different original lamellae orientations for uni-axial tension. Majority of pearlite colonies

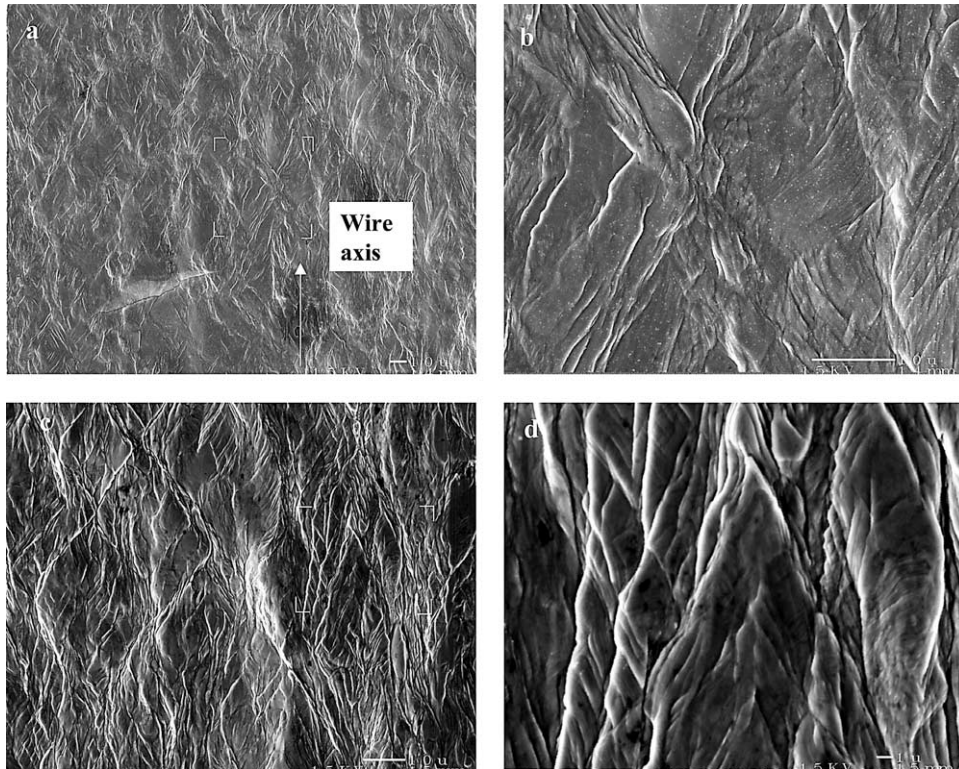


Fig. 13. Localization of plastic flow during wire drawing. (b) and (d) show regions bracketed in (a) and (c) at high magnification. Bright lines are traces of dislocation slip appeared at the pre-polished wire surface after drawing. (a, b) 20% and (c, d) 60% drawing strain SEM.

are aligned along the wire direction at strain $\varepsilon = 2$ (at $\varepsilon=1.5$ in the case of plane strain deformation). Buckling of pearlite colonies with large α -angle values contributes to their alignment along the wire axis (Fig. 10c). As an example, Fig. 10(d) shows atomic force micrograph illustrating alignment of pearlite colonies along the wire axis at $\varepsilon = 2.5$.

Fig. 11(a) and 11(b) illustrate a typical for pearlitic steels dependence of reduction of area, R.A., and torsion number before failure in a torsion test, N , as a function of drawing strain, respectively. Both R.A., a parameter characterizing local ductility, and N are reaching maximum at strain around of 1.5...2. The observed increase in R.A. and N at strain $\varepsilon < 2$ can be related to the fact that stress concentration at interfaces between colonies and accommodation deformation providing compatibility of their deformation decrease when lamellae

become oriented along the wire axis. Decrease in R.A. and torsion number at strains $\varepsilon > 2$ can be attributed to a number of factors, among which high elastic stresses at lamellar interfaces and strain localization accompanied by breaking up of pearlite plates may be the most important. Note that Aernoudt [20] related maximum in electric conductivity observed at $\varepsilon = 2$ to the alignment of ferrite lamellae.

Mechanism of re-orientation of pearlite colonies can be directly linked to dislocation slip. Operation of dislocation slip systems, localized shear, and buckling of lamellae result in colony rotation. Additionally to rotation of lamellae towards to the wire axis, development of [110] fiber texture can result in lamellae rotation around their own axis. Corresponding changes in γ -angle value are determined by Eq. (6c).

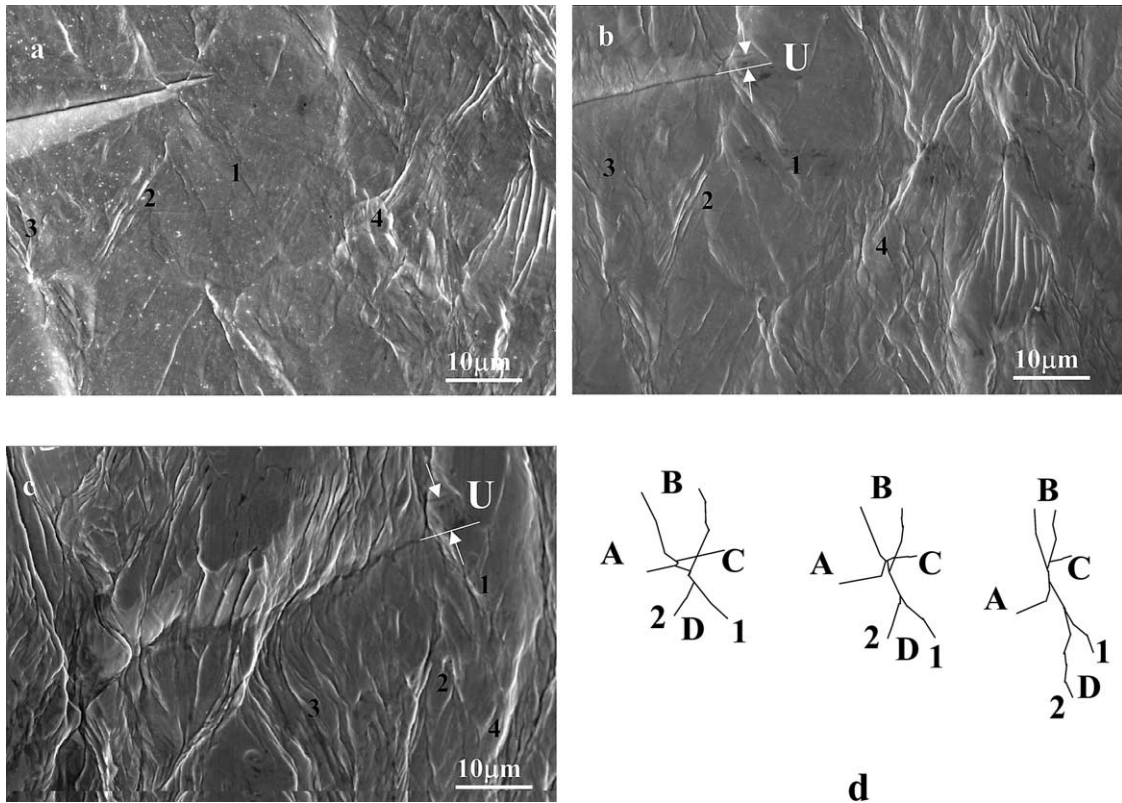


Fig. 14. The same region of a pearlitic wire at drawing strains of (a) 20%, (b) 40%, and (c) 60%. (d) is a schematic diagram illustrating shear surfaces indicated by numerals 1 and 2 and regions shearing with respect to each other shown by letters from A through D at consecutive strain levels. SEM.

5.2. Crystallographic texture

It is well documented that an axial $[110]$ -type texture develops during wire drawing of pearlitic steels. Work performed on relatively large diameter wires [38] indicates that $[110]$ fiber texture results in an alignment of (001) planes, which are cleavage planes in ferrite, along wire axis. Contiguous cleavage surface facilitates crack propagation causing wire break. Heizmann et al. [11] reported that a cyclic texture can also develop in the surface layers and at the wire center, possibly, also contributing to delamination under torsion loading.

Development of a strong crystallographic texture results in anisotropic mechanical properties. As an example, Fig. 12(a), (b) and (c) show indentations imprinted on a surface of as-patented wire and

drawn pearlitic steel by using a cone indenter and a Knoop diamond indenter, respectively. Microhardness is 900 HK in a normal direction and 760 HK along the wire axis (Fig. 12c). This difference in micro-hardness can be attributed to a larger number of interlamellar interfaces acting as barriers for dislocation movement in a normal direction as compared with axial direction. Despite this, a long axis of a cone indentation is parallel to the normal direction (Fig. 12b). Such an anisotropic behavior is consistent with that observed during wire rolling. Heavily drawn wires show lower elongation and larger radial flow as compared to an undeformed wire subjected to the same deformation. This can be related to operation of two other close packed directions resulting in the radial material flow in a $[110]$ -textured wire under compressive loading (Fig. 5b).

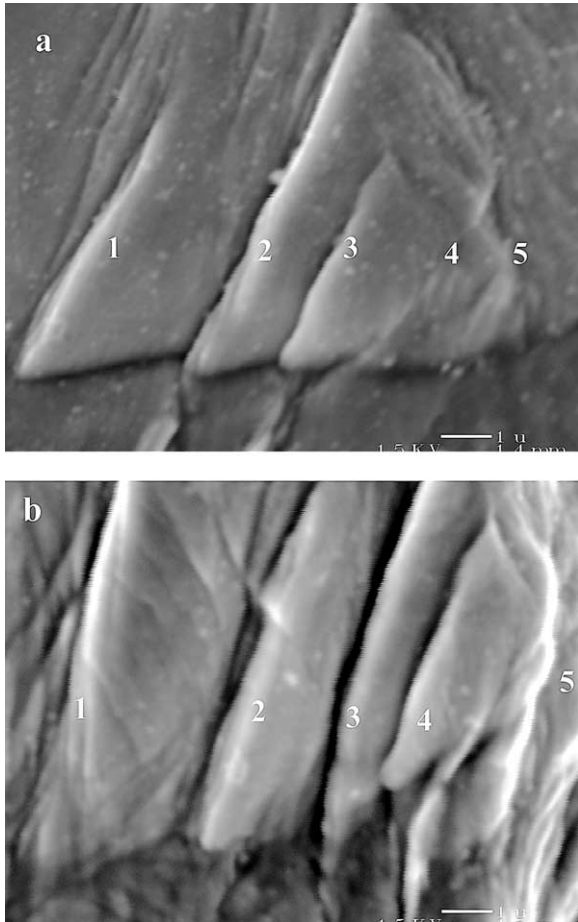


Fig. 15. The same fine slip surfaces (shown by numerals from 1 through 5) at the level of a pearlite colony after drawing to (a) 20% and (b) 40%. SEM.

6. Inhomogeneity of plastic flow

Fig. 13(a) and (b) show the same region of a pearlitic wire after drawing strain of 20% at different magnifications. Bright lines represent traces of dislocation slip surfaces. There are two systems of macroscopic shear bands (Fig. 13a) that is consistent with observations performed in eutectoid steel [39]. Angle between the macroscopic shear bands and wire axis is between 30 and 45 degrees. Traces of dislocation slip are clearly observed at higher magnification (Fig. 13b). At the initial drawing strain, slip lines are rather regularly distributed along the wire axis with spacing comparable to the

former austenite grain size. Slip lines form wedge-like features. With increasing drawing strain, length of the sides forming wedge-like features increases until the whole surface is divided into diamond-like cells (Fig. 13c). Traces of dislocation slip systems are seen within the cells at higher magnification (Fig. 13d).

Targeted observations performed at the same region at successive strain levels showed that even though new shear surfaces appear with increasing strain, deformation is localized at the same shear surfaces. Figs. 14 and 15 illustrate this fact at the scale of a former austenite grain size and a pearlite colony, respectively. The same coarse slip surfaces numbered from 1 through 4 in Fig. 14(a–c) and fine slip surfaces numbered from 1 through 5 in Fig. 15(a, b) are observed at successive strain levels indicating persistent strain localization. Schematics shown in Fig. 14(d) depict re-arrangement of regions indicated by letters A through D due to operation of shear surfaces 1 and 2. Regions B and D are moving apart from each other, while regions A and C are moving towards each other. This occurs due to stretching of these regions and their respective shear. Local shear, U , along shear surface 1 in Fig. 14(b) and (c) increases with drawing strain and is approximately $U = 5 \mu\text{m}$ at $\epsilon = 60\%$. For the shear band width of $2 \mu\text{m}$ this yields shear strain of 2.5 that is consistent with results of FEM modeling of drawing deformation at the scale of pearlite colony (Fig. 16a, b). Modeling showed tendency to strain localization in a form of shear bands for both longitudinal (Fig. 16a) and normal to the wire axis (Fig. 16b) orientation of pearlite lamellae. Atomic force micrograph shown in Fig. 16(c) supports occurrence of such a shear band cutting through ferrite/cementite plates.

Inhomogeneity of plastic flow during wire drawing can explain observed almost three fold decrease in total elongation even after small drawing strains (Fig. 17a). Interestingly, such a dramatic decrease in the overall tensile ductility occurs while local ductility characterized by the R.A.-values (Fig. 12a) increases (at strains less than 2). Overall macroscopic strain, ϵ , is determined by the local ductility, ϵ_1 , and length of the gauge portion in which deformation is localized, l :

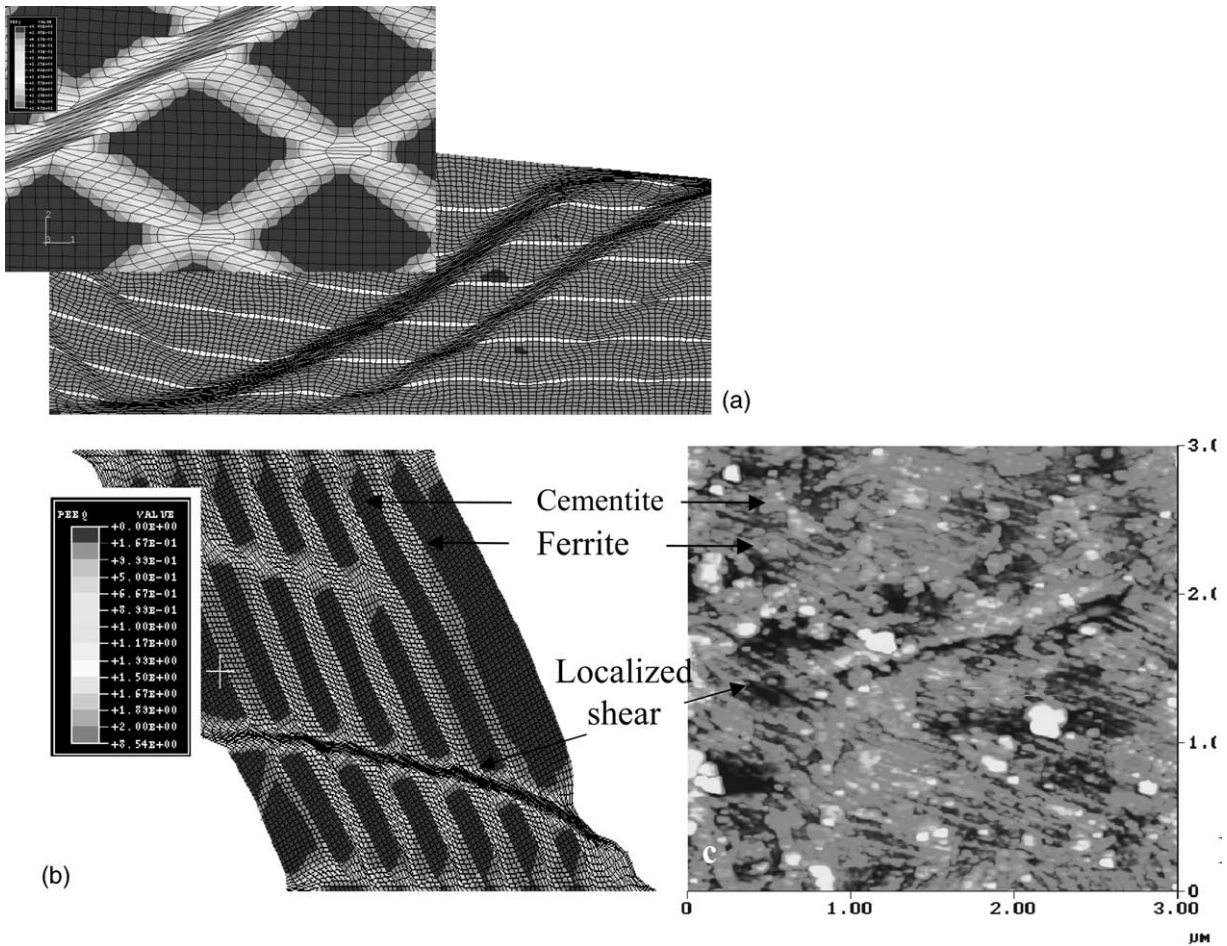


Fig. 16. FEM modeling results showing localized shear in a pearlite with ferrite/cementite plates orientated (a) parallel and (b) perpendicular to the wire axis, and (c) atomic force micrograph illustrating localized shear in a pearlitic steel.

$$\epsilon = l/L\epsilon_l \quad (7)$$

Here L is the total gauge length, and it is assumed for simplicity that deformation is localized only in one region and is distributed along the length of the localized region uniformly.

Decreasing total elongation while ϵ_l is increasing indicates a significant decrease in l -value. Such a decrease in material volume involved into deformation can be attributed to the existence of macroscopic shear surfaces established during wire drawing. These shear surfaces can be activated under tensile load leading to strain localization.

Special experiments performed on samples with different gauge length also indicated strain localiz-

ation as an important factor controlling overall elongation. Elongation to failure decreased with increasing gauge length (Fig. 17b) while the reduction area (illustrated by the insert given in Fig. 17b) was approximately 50% for all gauge lengths. Estimates of l/L -value based on these experiments indicate that only around 12 and 20% of the deformed volume is involved in actual deformation for samples with 250 and 80 mm gauge length, respectively.

7. Dynamic aging

Dissolution of cementite observed during wire drawing has been attributed to dragging of carbon

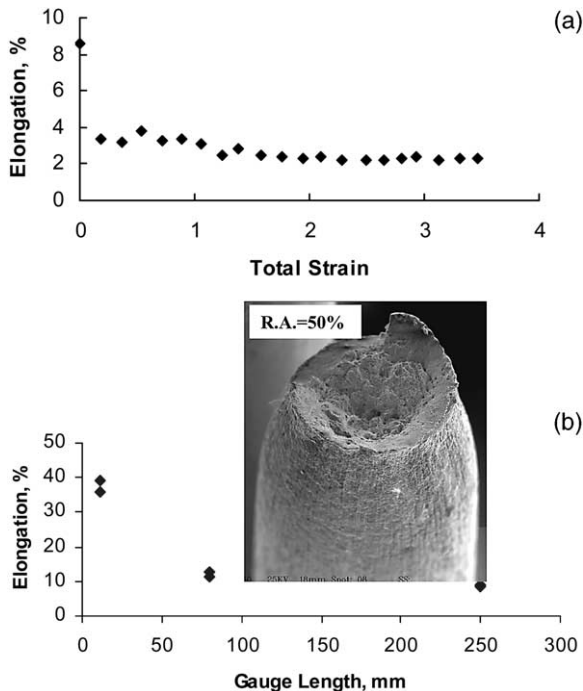


Fig. 17. (a) Typical for drawn pearlitic steels elongation to failure as a function of total drawing strain and (b) as a function of a sample gauge length. Insert in (b) shows an example of necking and area reduction in a sample with a 250 mm gauge length. SEM.

atoms by the ferrite dislocations crossing cementite lamellae [14,17]. This results in over-saturation of ferrite by carbon atoms. Adiabatic heat caused by plastic deformation can increase wire temperature up to 150...250 °C causing dynamic aging. Hono et al. [22] reported a complete dissolution of cementite plates and carbon atoms over-saturation in a wire drawn up to strain of 5.1. Assuming that lamellae thickness decreases according to the uni-axial law, estimated thickness of cementite lamellae is only 0.8 nm. Such a small thickness of cementite plates of only a few atomic layers will facilitate their dissolution.

Aging is accompanied by an approximately 5% strength increase (Fig. 18a) and ductility decrease (Fig. 18b), including increased susceptibility to delamination. Fig. 18(c,d) illustrate reduced torsion ductility due to aging on the example of wires drawn with different speed. Wire drawn with a low drawing speed did not delaminate (Fig. 18c).

Higher drawing speed yields higher wire temperature that accelerates aging causing delamination (Fig. 18d). Differential scanning calorimetry (DSC) showed that in delaminated wires peak on the DSC-curve (Fig. 19) corresponding to the temperature of 150 to 175 °C and attributed to formation of ϵ -carbides is smaller than that in non-delaminated wires. This suggests formation of ϵ -carbides during drawing due to dynamic aging in delaminated wires. Note that aging due to dislocations locking by nitrogen atoms can also affect properties of drawn steel.

8. Summary

Major process of microstructural evolution occurring during wire drawing of pearlite have been considered:

8.1. Lamellae thinning

- Thickness of ferrite and cementite lamellae decreases to a few nanometers in a heavily drawn wire.
- Predictions of lamellae thinning based on assumptions of uni-axial stretching are in a good consistency with measurements of inter-lamellar spacing and thickness of ferrite and cementite plates.
- Discrepancy between uni-axial manner of thinning of ferrite/cementite lamellae and their wavy appearance on a normal cross sections suggesting plane strain deformation can be related to lamellae bending along their long axis and deformation as a unit of pearlite colonies formed within a former austenite grain.

8.2. Evolution of interlamellar interfaces

- Surface area and volume fraction of ferrite/cementite interfaces significantly increases due to stretching of pearlite colonies and is comparable to that of cementite.
- Orientation of ferrite/cementite interfaces deviates from that corresponding to special orientation relationships.
- High elastic stresses are associated with

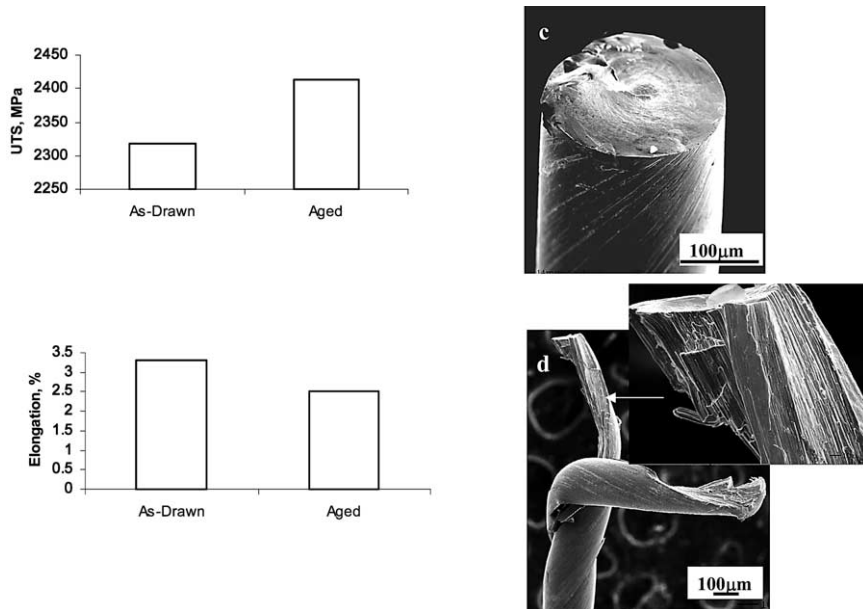


Fig. 18. (a) Ultimate tensile strength and (b) elongation to failure of as-drawn and aged pearlitic wires. (c) Delaminated and (d) non-delaminated under torsion loading pearlitic wires drawn with a slow speed and high speed, respectively. SEM.

ferrite/cementite interfaces contributing to brittleness of highly drawn steel. Region affected by the high elastic stresses is approximately 0.1 of lamellae thickness.

8.3. Texture development

- Metallographic texture, highly elongated pearlite colonies aligned with the wire axis, is formed after drawing strain of from 1.5 to 2.
- Increase in local ductility of pearlitic wires characterized by the reduction area, R.A., with increasing drawing strain from 1.5 to 2 can be related to lower stress concentration between aligned pearlitic colonies. Decrease in R.A. with further increasing drawing strain can be related to strain localization and breaking up of cementite lamellae.
- Crystallographic texture causes 20% higher strength in the radial direction as compared to that in axial direction and lower elongation and larger spread during wire rolling.

8.4. Localized plastic flow

- Plastic deformation during wire drawing is non-uniform. Two systems of localized shear bands formed by coarse slip and fine slip surfaces orientated under from 30 to 45 degrees with respect to the wire axis are observed.
- Targeted observations performed from the same region at successive strain levels showed wedge-like features formed by the surfaces of localized shear at the initial strain stages. These shear surfaces develop into macroscopic shear bands propagating through the entire wire cross-section.
- Localized shear bands divide material into cells with size comparable with the size of former austenite grains. Spacing of localized shear bands decreases with increasing drawing strain.

8.5. Dynamic aging

- Large plastic deformation can cause cementite dissolution leading to ferrite oversaturation with

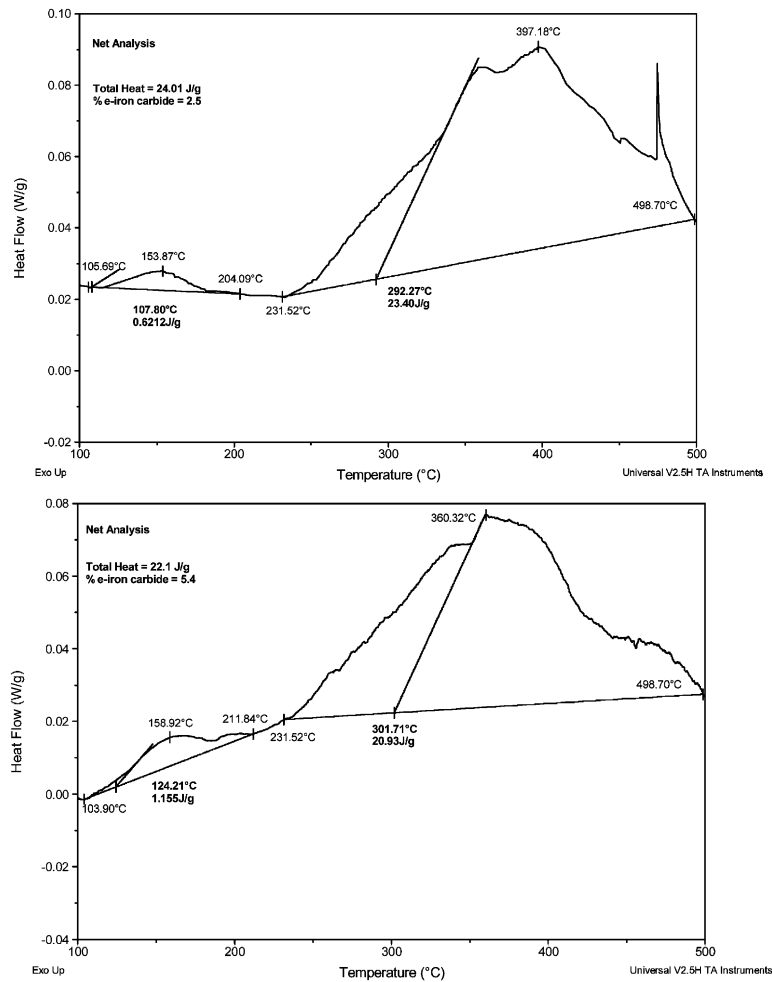


Fig. 19. DSC spectra obtained from (a) non-delaminated filament and (b) delaminated filament.

carbon atoms that in combination with adiabatic heating results in aging increasing strength by up to 5–6%.

- Aging promotes delamination, wire axial cracking under torsion loading.

Acknowledgements

Help with conducting of wire drawing experiments and microstructural characterization of Mr S. Babbo, J. Lewis, and W. Lewis is greatly appreciated, as well as useful discussions with Dr A. Prakash, Dr D. Kim, and Mr T. Starinshak.

Author is also grateful to Nippon Steel Co. and Sumitomo Metal Industries Ltd for permission to use data, and Goodyear Tire & Rubber Co. for permission to publish the data.

References

- [1] Embury JD, Fisher RM. Acta Metall 1966;14:147.
- [2] Chandhok VK, Kasak A, Hirth JP. Trans ASM 1966;59:288.
- [3] Glenn RC, Langford G, Keh AS. Trans ASM 1969;62:285.
- [4] Langford G. Metall Trans 1970;1:465.
- [5] Langford G. Metall Trans 1977;8A:861.

- [6] Aernoudt E, Sevillano JS. *J Iron Steel Inst* 1973;211:718.
- [7] Gil Sevillano J, Van Houtte P, Aernoudt E. *Progr Mater Sci* 1980;25:69.
- [8] Dollar M, Bernstein IM, Thompson AW. *Acta Metall* 1988;36:311.
- [9] Pilarczyk JW, Van Houtte P, Aernoudt E. *Mater Sci Eng* 1995;A197:97.
- [10] Hallgarth JK. *Ironmaking and Steelmaking* 1995;22:211.
- [11] Montesin T, Heizmann JJ, Abdellaoui A, Pelletier JB. *Wire J Int* 1993;4:163.
- [12] Lesuer DR, Syn CK, Sherby OD, Kim DK. Processing and mechanical behavior of hypereutectoid steel wires. In: Paris HG, Kim DK, editors. *Metallurgy, Processing and Applications of Metal Wires*. Warrendale, PA: TMS; 1996.
- [13] Van Acker K, Root J, Van Houtte P, Aernoudt E. *Acta Mater* 1996;44:4039.
- [14] Watte P, Van Humbeeck J, Aernoudt E, Lefever I. *Scr Mater* 1996;34:89.
- [15] Languillaume J, Kapelski G, Baudelet B. *Acta Mater* 1997;45:1201.
- [16] Makii K, Yaguchi H, Ibaraki N, Miyamoto Y, Oki Y. *Scr Mater* 1997;37:1753.
- [17] Danoix F, Julien D, Sauvage X, Copreaux J. *Mater Sci Eng* 1998;A250:8.
- [18] Toribio J, Ovejero E. *Scr Mater* 1998;39:323.
- [19] Hong MH, Reynolds Jr. WT, Tarui T, Hono K. *Metall Mater Trans* 1999;A30:717.
- [20] Aernoudt E. *Wire J Int* 2000;12:97.
- [21] Geltkov AC, Filippov VV. *Steel* 2001;2:45.
- [22] Hono K, Ohnuma M, Murayama M, Nishida S, Yoshie A, Takahashi T. *Scr Mater* 2001;44:977.
- [23] Ibaraki, N., Makii, K., Ochiai, K., Oki, Y., 1999. Wire rods for ultra tensile steel cord. In: *Proc. of 69th Wire & Cable Technical Symposium*, Guilford, USA: The Wire Assoc Intl, p. 1.
- [24] Starinshak TW, Shemenski RM, Hammer G. *Wire J Int* 1988;21:45.
- [25] Paris HG, Kim DK, editors. *Metallurgy, Processing and Applications of Metal Wires*. Warrendale, PA: TMS; 1996.
- [26] Delrue, H., Bruneel, E., Van Humbeeck, J., Aernoudt, E., 2000. Atomic Force Microscopy: a powerful tool to study the radial gradients in mechanical properties of hard-drawn pearlitic steel wire. In: *Proc. of 70th Wire & Cable Technical Symposium*, Guilford, USA: The Wire Assoc. Intl., p. 5.
- [27] Hosford Jr. WF. *Trans ASM-AIME* 1964;230:12.
- [28] Courtesy of Dr Tashiro H., 1999. Nippon Steel Co.
- [29] Zhou S, Shiflet GJ. *Metall Trans* 1992;23A:1259.
- [30] Courtesy Mr Taniyama T. Sumitomo, 1999. Metals Ind.
- [31] Fortes MA, Ferro AC. *Acta Metall* 1985;33:1697.
- [32] Hall EO. *Proc Phys Soc B* 1951;64:747.
- [33] Petch NJ. *J Iron Steel Inst* 1953;174:25.
- [34] Hidaka H, Tsuchiyama T, Takaki S. *Scr Mater* 2001;44:1503.
- [35] Whiting MJ, Tsakiroopoulos P. *Mater Sci Technol* 1995;11:717.
- [36] Zelin, M., *Acta mater.* 2002, to be submitted.
- [37] US Patent 5,189,897.
- [38] Shimizu, K., Kawabe, N., 2001. Fracture mechanics aspects of delamination occurrence in high-carbon steel wire. In: *Proc. of 71st Wire & Cable Technical Symposium*, Guilford, USA: The Wire Assoc Intl, p. 35.
- [39] Korbel A, Bochniak W, Ciura F, Dybiec H, Piela K. *J Mater Proc. Technol* 1998;78:104.